Subject-specific real-time respiratory liver motion compensation method for ultrasound-MRI/CT fusion imaging

Article *in* International Journal of Computer Assisted Radiology and Surgery · June 2014

DOI: 10.1007/s11548-014-1085-x · Source: PubMed

CITATIONS
5

READS
132

5 authors, including:

Minglei Yang
Tsinghua University
11 PUBLICATIONS **18** CITATIONS
SEE PROFILE

Hui Ding
Tsinghua University
66 PUBLICATIONS **159** CITATIONS
SEE PROFILE

Guangzhi Wang
Tsinghua University
240 PUBLICATIONS **666** CITATIONS
SEE PROFILE

Int J CARS (2015) 10:517–529
DOI 10.1007/s11548-014-1085-x

ORIGINAL ARTICLE

Subject-specific real-time respiratory liver motion compensation method for ultrasound-MRI/CT fusion imaging

Minglei Yang · Hui Ding · Jingang Kang · Lei Zhu · Guangzhi Wang

Received: 10 January 2014 / Accepted: 29 May 2014 / Published online: 14 June 2014

Abstract
Purpose Ultrasound-MRI/CT fusion imaging is widely used in minimal invasive surgeries, such as liver biopsy and tumor ablation. However, respiration-induced quasi-periodic liver motion and deformation cause unacceptable misalignment of the fusion images (i.e., fusion error). A subject-specific liver motion model based on skin-mounted position sensor and corresponding ultrasound liver image sequence was developed to compensate for liver motion.
Methods External surrogate respiratory motion signal is used to predict internal liver motion. An electromagnetic position sensor fixed on abdominal skin is introduced to track the respiratory motion, and 2D ultrasound images are used to track the liver motion synchronously. Based on these measurements, a subject-specific model describing the relationship of respiratory skin motion and internal liver motion is built and applied in real time (ultrasound-MRI/CT fusion imaging system) to predict and to compensate for the liver motion due to respiratory movement. Feasibility experiments and clinical trials were carried out on a phantom and eight volunteers.
Results Qualitative and quantitative analyses and visual inspections performed by experienced clinicians show that the proposed model could effectively compensate for the liver motion, and the ratio of motion-compensated fusion error to the original varied from 10 % (0.96/9.40 mm) to 28 % (2.90/10.22 mm).
Conclusions An online liver motion modeling and compensation method was developed that provides surgeons with stable and accurate multimodality fusion images in real time.

Keywords Ultrasound-MRI/CT fusion imaging · Respiratory liver motion · Fusion errors · Real-time motion compensation

M. Yang · H. Ding · G. Wang (✉)
Department of Biomedical Engineering, School of Medicine, Tsinghua University, Room C249, Beijing 100084, People's Republic of China
e-mail: wgz-dea@tsinghua.edu.cn

M. Yang
e-mail: yangml122@gmail.com

H. Ding
e-mail: dinghui@tsinghua.edu.cn

J. Kang · L. Zhu
Beijing Shen Mindray Medical Electronics Technology Research Institute Co. Ltd, 3F, Building 5, No. 8 Chuangye Road, Shangdi Haidian District, Beijing 100085, People's Republic of China
e-mail: kangjingang@mindray.com

L. Zhu
e-mail: zhulei@mindray.com

Introduction

Ultrasound-MRI/CT fusion imaging technique [1] fuses pre-acquired three-dimensional (3D) images, such as magnetic resonance images (MRI) and computed tomography (CT) images, with intra-operative two-dimensional (2D) ultrasound images to take advantage of both high spatial resolution of 3D dataset and high temporal resolution of real-time 2D imaging. Moreover, the fusion image overcomes the disadvantages of ultrasound imaging such as poor image quality and low capability in lesion identification [2–4]. Therefore, fusion image can provide surgeons with supplementary information during noninvasive diagnosis, minimal invasive surgery and postoperative evaluation [5–8]. However, due to liver motion and deformation induced by respiration, unacceptable misalignment of fusion images (i.e., fusion error) makes it hard to register images perfectly in a longitudinal study [9].

Clinically, respiratory gating [10], active breathing control [11,12], anesthesia with jet ventilation [13], and X-ray tracking with or without implanted fiducials [14,15] were conventionally adopted in liver biopsies and tumor ablation surgeries to correct the targeted lesion motion caused by respiration. Hakime et al. [16] showed that electromagnetic needle tracking improved liver biopsy efficiency. Currently, ultrasound-MRI/CT fusion imaging devices [17–21] carry out quasi-static fusion imaging using a respiratory gating-like approach. In our previous work [22], preoperative 3D images were acquired while subject held breath at half expiration. 2D ultrasound images used to perform registration were acquired at the same respiratory phase. After ultrasound images and MRI/CT images were co-registered, images from different modalities were fused in real time. However, the effectiveness and accuracy of the fusion information could only be obtained near the respiratory phase of registration. As a matter of fact, the fusion errors were unacceptable for most part of the breathing cycle. Accordingly, the subject had to hold breath many times at the same respiratory phase (half expiration). Therefore, quasi-static fusion imaging was limited in practice since it required subject's cooperation during multiple breath holds. It also greatly prolonged operating time and decreased operation effectiveness.

Many researchers proposed to build four-dimensional (4D, i.e. 3D+time) model to depict the respiration-induced spatial movement and deformation of liver and to compensate for it in minimal invasive surgeries/therapies [23–26]. However, 4D model required expensive 4D MRI/CT dataset and complicated modeling processes, which was time-consuming. Meanwhile, poor real-time capability and significant individual variations of 4D model limited its clinical application. Consequently, some methods without using 4D model were investigated in the past few years. Atkinson et al. [27] used a 1D translation model to describe the respiratory motion of heart, and to correct the 3D spatial positions of cardiac images. This simple model improved the image quality of 3D freehand echocardiography. Xu et al. [6] and De Silva et al. [28] adopted a 2.5-dimensional (2.5D)/ 3D image registration method that registered 2.5D ultrasound images (several 2D image slices with known positions) and 3D MRI images in real time to track and compensate for the prostate motion in MRI-TRUS (transrectal ultrasound) fusion. However, this method compensated for the average motion of the 2.5D image set instead of the exact motion of the current ultrasound image frame. Wein et al. [29] tracked the patient's skin motion caused by respiration using a position sensor and obtained liver motion using slice to volume registration for ultrasound images. An affine model was then built to predict liver motion and reduce the fusion errors. This method performed slice to volume registration which was time-consuming. In addition, speckle noise and poor image quality of ultrasound image limited the accuracy of the registration.

Over the years, researchers have worked on simplified liver motion model. Blackall et al. [30] concluded that free breathing had good intra- and inter-cycle reproducibility across the tidal breathing range. Rofling et al. [31] and Brandner et al. [32] indicated that liver motion was mainly in the form of translation along the human SI (superior–inferior) axis. In our earlier work [33], we observed that respiration-induced liver motion were mainly in the form of rigid motion. A 2D sagittal plane translation motion model could compensate for liver motion by at least 80 %. Gierga et al. [34] and Ernst et al. [35] demonstrated that the motion of fiducials attached to patient skin and inner organs were greatly correlated, implying that internal liver motion could be predicted using skin surrogate motion signal. In addition, De Groote et al. [36] placed tracking markers on abdomen and showed that the largest abdominal skin displacement was at the umbilicus.

The purpose of this study was to develop an online subject-specific liver motion model to compensate for the liver motion caused by respiratory movement in real time. This method was validated on an abdominal phantom and eight volunteers. Qualitative and quantitative analyses and visual inspections were performed to evaluate whether the proposed model could effectively compensate for the liver motion and thereby reduce relevant fusion errors. The ultimate goal was to provide surgeons with stable multimodality fusion images with acceptable accuracy in real time.

Materials and methods

System overview

The ultrasound-MRI/CT fusion imaging system [22] used in this study consists of a medical ultrasound imaging equipment and an electromagnetic (EM) tracking system. The system tracks the ultrasound image plane using an EM position sensor attached to the ultrasound probe. The spatial relationship (Eq. 1) between intra-ultrasound images and pre-acquired 3D MRI/CT images is built upon 2D/3D registration. Images from different modalities are then fused and displayed in real time.

The fusion process involves the following coordinate systems: (1) ultrasound image coordinate system, labeled as 'us,' is defined in the ultrasound image plane; (2) EM position sensor coordinate system, labeled as 's,' is defined by the EM position sensor attached on the ultrasound probe; (3) world coordinate system, labeled as 'w,' is defined by the EM field generator; and (4) 3D images coordinate system, labeled as '3D,' is defined in 3D images. If we assume $\vec{x}_{\mathrm{us}}$ is an arbitrary point in ultrasound image plane, and $\vec{x}_{\mathrm{3D}}$ is the correspond-

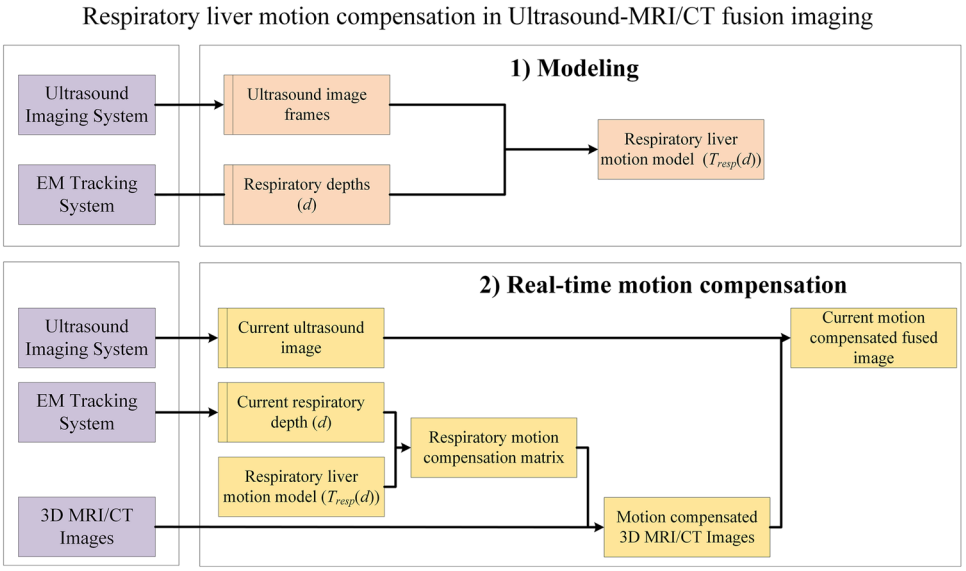

Fig. 1 Schematic diagram of respiratory liver motion compensation in ultrasound-MRI/CT fusion imaging. At the stage of modeling (Stage 1), a subject-specific model describing the relationship between respiratory motion signal and liver motion is established. This model is used to predict and compensate for liver motion in real-time fusion imaging (Stage 2), thereby reducing the fusion errors caused by respiratory movement

ing point in the 3D images, the transformation from $\vec{x}_{\text{us}}$ to $\vec{x}_{\text{3D}}$ can be expressed as follows [22]:

$$\vec{x}_{\text{3D}} = T_{\text{3D}\leftarrow w} \cdot T_{w\leftarrow s} \cdot T_{s\leftarrow \text{us}} \cdot \vec{x}_{\text{us}} \tag{1}$$

where $T_{s\leftarrow \text{us}}$ is the transformation from ultrasound image to EM position sensor coordinate system, which can be determined by calibration after the sensor is fixed on the ultrasound probe [22]. $T_{w\leftarrow s}$, the transformation from EM position sensor to world coordinate system, can be obtained directly from EM tracking system. $T_{\text{3D}\leftarrow w}$ performs the transformation from world coordinate system to 3D images coordinate system, which is determined through manual image registration based on liver structures in both ultrasound images and 3D MRI/CT images.

Based on the above rigid framework of this fusion system, a respiratory compensation matrix $T_{\text{resp}}(d)$ is added to Eq. 1 to compensate for the respiratory liver motion which causes misalignment of fusion images:

$$\vec{x}_{\text{3D}} = T_{\text{3D}\leftarrow w} \cdot T_{\text{resp}}(d) \cdot T_{w\leftarrow s} \cdot T_{s\leftarrow \text{us}} \cdot \vec{x}_{\text{us}} \tag{2}$$

where d indicates the respiratory motion signal (namely, respiratory depth) corresponding to current ultrasound image. If a subject-specific model $T_{\text{resp}}(d)$ is established, and the respiratory depth d is measured in real time, the respiratory liver motion can be corrected in real-time fusion imaging using Eq. 2.

To accomplish this, a two-stage procedure (Fig. 1) is designed to implement the liver motion compensation. At Stage 1, an online subject-specific respiratory liver motion model $T_{\text{resp}}(d)$, which maps the translation of abdomen skin to liver motion during smooth breathing, is built before images fusion. An additional EM position sensor attached to subject's abdominal skin tracks the respiratory depth d. Meanwhile, a sequence of 2D ultrasound image frames is captured to track the internal liver motion. Both measurements are then used to construct the respiratory liver motion model. This model is then applied in real-time fusion imaging (Stage 2) to predict liver displacement according to respiratory EM sensor's position. The current $T_{\text{resp}}(d)$ is used to compensate for liver motion, thereby reducing the corresponding fusion error.

Modeling

Previously, we demonstrated that a 2D sagittal plane translation model could correct the liver motion by at least 80 % [33]. In this study, the same model is employed to depict the subject-specific respiratory liver motion. External surrogate respiratory motion signal is used to predict internal liver motion.

As shown in Fig. 2, the position of respiratory EM sensor is used to generate the respiratory mapping function to measure respiratory depth. Then, the 2D ultrasound image frames are processed with a speckle tracking technique [37] to track the internal liver motion synchronously with each respiratory depth. For speckle tracking process, region of interest (ROI) is selected and then divided into several sub-blocks in the first frame to improve computational efficiency and reliability. Considering that there exist some invalid sub-blocks with marginal valuable feature information, a normalized histogram-based decision parameter is designed to discard these invalid sub-blocks. The sagittal in-plane liver motion obtained by speckle tracking is then mapped to the 3D world space. Eventually, a linear fitting model combines respiratory depth and internal liver motion to determine the subject-specific liver motion.

Respiratory mapping

The respiratory sensor is a 6 Degrees of freedom (Dof) EM position sensor. However, the motion of abdominal skin is mostly in the direction of dilation-contraction. Thus, Primary Component Analysis (PCA) [38] is applied to map the 3D respiratory sensor's position to a 1D respiratory depth along the first primary axis.

For convenience, the ultrasound image time sequence and the corresponding respiratory motion signals are labeled as 'UITS-RMS set.' The respiratory sensor position at moment t is denoted as $\overrightarrow{P_t} = (x_t, y_t, z_t)^T$, then the position time sequence in UITS-RMS set can be formulated as a matrix:

$$P = \left[\overrightarrow{P_1}, \overrightarrow{P_2}, \ldots \overrightarrow{P_t}, \ldots \overrightarrow{P_N}\right], \; t = 1, 2, \ldots, N \tag{3}$$

where N is the number of the respiratory sensor positions, i.e. the frames of the corresponding ultrasound image time sequence.

The first primary axis $\overrightarrow{A_p}$ is obtained by applying PCA method to P [38]. Then, the respiratory mapping function can be generated by:

$$d_t = f_d(\overrightarrow{P_t}) = \overrightarrow{A_p} \cdot \overrightarrow{P_t} \tag{4}$$

where d_t is the respiratory depth corresponding to current respiratory EM sensor's position.

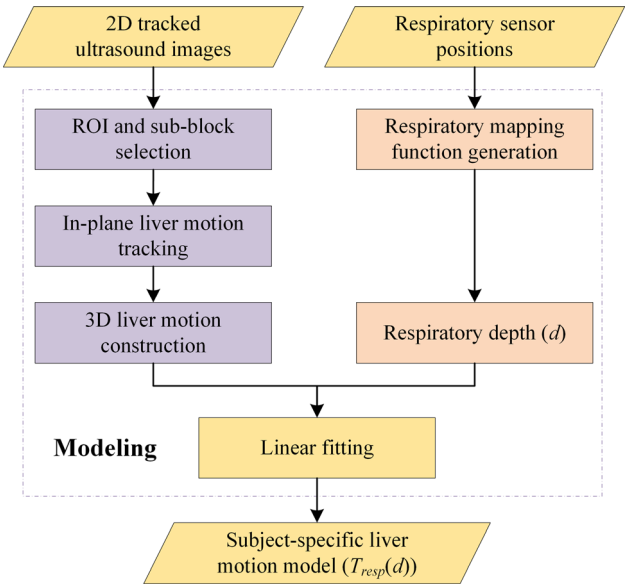

Fig. 2 Flow chart of subject-specific respiratory liver motion modeling. Liver motion is obtained from 2D ultrasound image frames using a speckle tracking method. Respiratory depth is measured synchronously with each ultrasound image frame. The liver motion model is then built using linear fitting

Liver motion tracking

Speckle tracking technique is employed on the sequential ultrasound image frames for several respiratory cycles to obtain the sagittal in-plane liver motion for each subject. Liver motion in the world coordinate is then calculated using Eq. 1. This process is divided into the following three steps (Fig. 2, left column):

(*1*) *ROI and sub-block selection* Compared to superficial skin and deep abdominal tissues, respiration-induced liver motion has its regularity. In addition, liver occupies only a small area in the sagittal liver ultrasound image (Figs. 3a, 4a). Therefore, we draw a ROI to include left liver only in the first frame of the ultrasound images. To make the computation more efficient, sub-blocks are defined within this ROI to further exclude the regions that contribute little information for tracking (Figs. 3a, 4a). Mathematically, a normalized histogram-based decision parameter F is designed to select the valid sub-blocks and discard the invalid sub-blocks, where $F = 1$ and $F = 0$ represent valid and non-valid sub-block, respectively. F can be determined as follows:

$$F = \begin{cases} 1, & I_t > I_\alpha \\ 0, & I_t \leq I_\alpha \end{cases} \tag{5}$$

where I_t is the information index of a sub-block, and I_α is the information index of the whole ultrasound image, indicating a global assessment of this image. I_t and I_α can be determined by:

$$I_t = \min_I \left\{ I \left| cdf_{H(s)}(I) > r_t \right. \right\} \tag{6}$$

$$I_\alpha = \alpha(I_{\max} - I_{\min}) + I_{\min} \tag{7}$$

where I_t is the smallest intensity in $\left\{ I \left| cdf_{H(s)}(I) > r_t \right. \right\}$. $H(s)$ is the normalized histogram of a sub-block s in ROI. $cdf_{H(s)}$ means the cumulative distribution of $H(s)$. $I_{\min}$ and $I_{\max}$ donate the minimum and maximum intensity in the whole ultrasound image. α donates the ratio of pixels whose intensity is lower than intensity I_α. In this study, α was 0.3, r_t was 0.7, and the bin size of the histogram was 20.

(*2*) *Inter-frame liver motion tracking* On high frame rate (approximately 10 frames/s) ultrasound images, liver moves slightly between frames (approximately 1 mm) [32,33]. This makes it feasible to track liver motion using speckle tracking technique, which is implemented based on block matching [39]. By optimizing normalized cross-correlation coefficient (NCC) between valid sub-blocks sets in adjacent frames, the liver motion $\vec{v}(I_i, I_{i+1})$ from ith to $(i+1)$th ultrasound image frame is determined (Figs. 3b, 4b).

(*3*) *3D Space liver motion construction* The inter-frame liver motion $\vec{v}(I_i, I_{i+1})$ is a 2D motion in ultrasound imaging

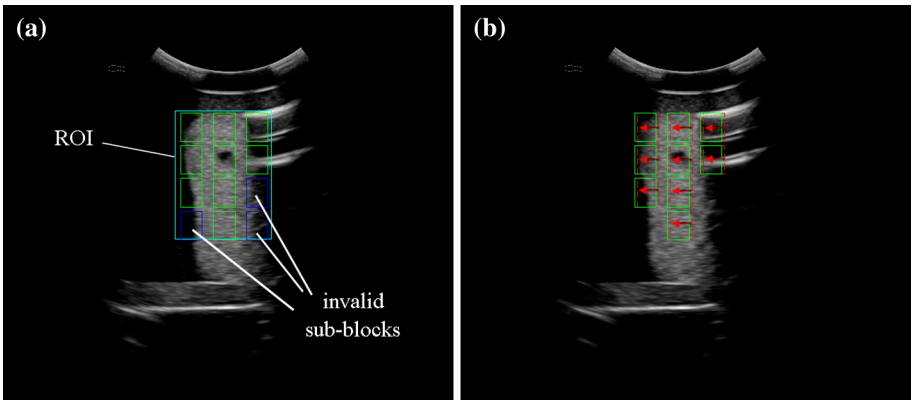

Fig. 3 Liver motion tracking in respiration simulation study using a phantom. **a** Whole ROI (*largest rectangle*) and sub-blocks in the first frame of ultrasound image time sequence, where *small green rectangles* represent the valid sub-blocks, and small blue rectangles are the invalid ones. **b** Motion tracking using speckle tracking technique, where *red dashed rectangles* indicate the liver phantom position in (**a**), i.e. previous frame, *green solid rectangles* demonstrate the phantom position in current frame, and the *red arrows* show the inter-frame phantom motion

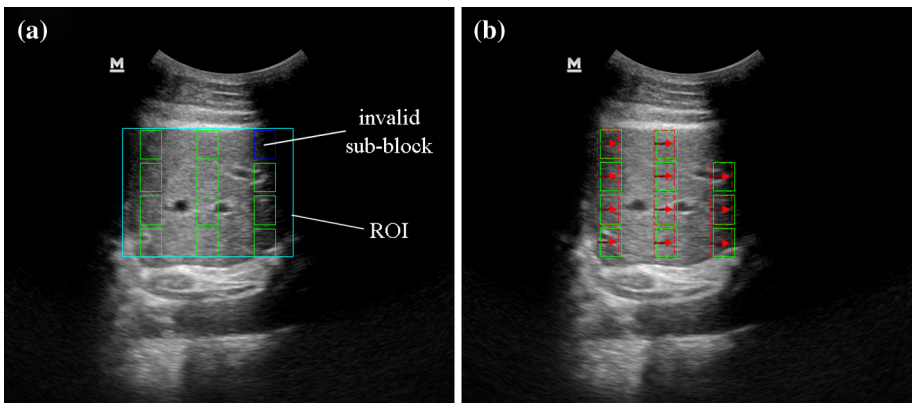

Fig. 4 A typical liver motion tracking in clinical study. **a** Whole ROI and sub-blocks in the first frame of ultrasound image time sequence, using the same definition as Fig. 3. **b** Motion tracking of liver using speckle tracking technique, where red arrows indicate the inter-frame motion of the valid sub-blocks in liver

plane, which can be mapped to 3D world coordinate system using:

$$\vec{v}_w = T_{w\leftarrow s} \cdot T_{s\leftarrow \mathrm{us}} \cdot \vec{v}_{\mathrm{us}} \tag{8}$$

Liver motion during several breathing cycles in 3D is then obtained. Inevitably, the handheld probe incurs some translation and rotation while the UITS-RMS set is captured. Using Eq. 8, translation and rotation of the probe is corrected through the tracked probe information synchronously.

Model construction

A linear model is used to define the subject-specific liver motion:

$$\vec{v}_w = f_{xyz}(d) = \vec{a}_1 \cdot d + \vec{a}_0 \tag{9}$$

where $\vec{v}_w = (v_x, v_y, v_z)^T$ is the liver motion vector in the world coordinate system, d is the respiratory depth. $\overrightarrow{a_1}$ and $\overrightarrow{a_0}$ are determined using linear fitting.

Real-time motion compensation

Once the subject-specific liver motion model is built, ultrasound images are manually registered to 3D MRI/CT images by an experienced clinician. The position of respiratory EM sensor $\overrightarrow{P_{\mathrm{reg}}}$ at the time of registration is recorded. The corresponding respiratory depth d_{reg} is calculated using Eq. 4. Thereafter, the liver motion vector $\overrightarrow{v_{\mathrm{reg}}} = f_{xyz}(d_{\mathrm{reg}})$ is obtained from Eq. 9.

At the stage of real-time fusion imaging, the current respiratory sensor position is captured synchronously with current ultrasound image. Respiratory depth $d_t = f_d(\overrightarrow{P_t})$ and corresponding liver motion vector $\overrightarrow{v_t} = f_{xyz}(d_t)$ are obtained to determine the compensation vector:

$$\overrightarrow{v_{t_{\mathrm{com}}}} = \overrightarrow{v_t} - \overrightarrow{v_{\mathrm{reg}}} = (v_{x_{\mathrm{com}}}, v_{y_{\mathrm{com}}}, v_{z_{\mathrm{com}}}) \tag{10}$$

Then $T_{\mathrm{resp}}(d)$ calculated in Eq. 11 is applied to Eq. 2 to transform the coordinates of the pixels in currently scanned ultrasound image to the 3D MRI/CT images space. The

corresponding liver information in MRI/CT images is then extracted to form a MRI/CT slice based on these transformed coordinates. At last, the MRI/CT slice is fused with the ultrasound image and displayed to clinician. Since skin and liver movements vary from subject to subject, the proposed model built for one individual cannot be generalized to another. Therefore, the model should be constructed and applied specifically for each subject.

$$T_{\text{resp}}(d) = \begin{bmatrix} 1 & 0 & 0 & -v_{x_{\text{com}}} \\ 0 & 1 & 0 & -v_{y_{\text{com}}} \\ 0 & 0 & 1 & -v_{z_{\text{com}}} \\ 0 & 0 & 0 & 1 \end{bmatrix} \tag{11}$$

At the stage of real-time fusion imaging, the liver motion model is used to predict and compensate for liver motion frame by frame. The ultrasound device in our experiments displayed fused images at a frame rate of 10–15 frames/s (0.067–0.1 second per frame) with respiratory motion compensated.

Evaluations and experiments

Equipment and MRI/CT datasets

3D CT dataset in phantom study was obtained using Somatom Sensation 16 (Siemens Healthcare, Germany). The spacing between slices was 0.7 mm and the pixel spacing was 0.64 mm × 0.64 mm.

Abdominal 3D MRI dataset in clinical study were acquired on a 3.0T whole-body MR scanner (Achieva TX, Philips Medical System, Best, the Netherlands) when subjects held breath at half expiration in supine position. Slice thickness was 4 mm with 2 mm gap. In-plane pixel size was 1.36 mm × 1.36 mm. Total scan time was about 15 s.

Ultrasound image was captured using a DC8 Color Doppler Ultrasound System (Mindray Co., Ltd, Shenzhen, China). The pixel spacing was 0.30 mm × 0.30 mm. And the image plane was tracked using a 6 Dof EM position sensor attached to the ultrasound probe. The respiratory motion signal was obtained by another 6 Dof EM position sensor placed on abdominal skin. Position of both sensors were tracked by the Aurora Electromagnetic Tracking System (Northern Digital Inc., Canada).

Phantom study

Phantom study (Fig. 5) was performed to evaluate the performance of the proposed liver motion prediction model qualitatively and quantitatively.

The abdominal phantom (D-5658-1, CIRS Inc., USA) was fixed on a PMMA (polymethyl methacrylate) tray. The tray was constrained by a pathway to move horizontally in one direction. The tray and its pedestal were fixed on the experiment table. To simulate the respiratory liver motion, the tray holding the phantom was driven by a robot arm (VP-6242G, Denso Inc., Japan) to move along the pathway back and forth quasi-periodically. The phantom position y along the pathway at time t was determined by:

$$y = (A + \delta A) \sin\left(\frac{2\pi}{T + \delta T} t + \frac{\pi}{4}\right) \tag{12}$$

where A and δA were the amplitude and the random disturbance for different cycles. T and δT were the motion period and the random disturbance for each cycle. Normal human breathing cycle is about 2 s, and liver motion along SI axis is about 10–20 mm [32]. Therefore, $A = 14\,\text{mm}, \delta A \leqq 2\,\text{mm}, T = 2\,\text{s}, \delta T \leqq 0.2\,\text{s}$ were used, which limited the fusion error to 32 mm at most.

EM field generator was placed on one side of the phantom and was kept far away from the metal robot arm to reduce

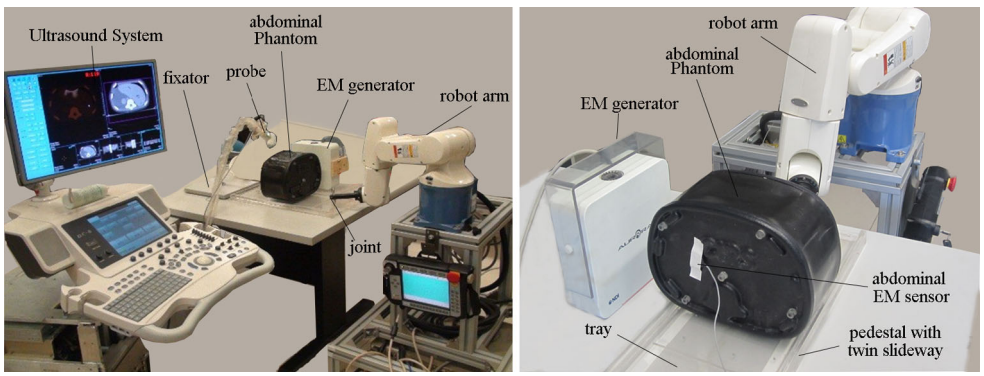

Fig. 5 Setup of phantom study. The abdominal phantom was fixed on a PMMA tray, which was constrained by a pathway. The pathway and its pedestal were fixed on the experiment table. Then, the tray holding the phantom was driven to move horizontally along the pathway by a robot arm to simulate the respiratory liver motion

its interference to the EM field. An EM position sensor was attached to one side of phantom to track the simulated respiratory skin motion. And it was also used to track the true phantom position in order to validate the accuracy of liver motion prediction using the proposed model.

In our primary work, the UITS-RMS set was captured when the ultrasound probe was attached to an external fixator (FEF). Four different simulations were then designed, in which UITS-RMS sets were captured when the probe was: (1) handheld steadily (HHS), (2) handheld and rotated around phantom SI axis (HHR-SI), (3) handheld and rotated around AP axis (HHR-AP), and (4) handheld and translated with random rotation (HHTRR). Five motion models were built, respectively.

After the ultrasound images were aligned to the CT images of the phantom, the models were used to predict and to compensate for the simulated liver motion. On the fused images, clinician visually compared the consistency of identical structures, such as liver capsule and vessels, with/without motion compensation to assess the model performance in real-time fusion imaging. Quantitative analysis was also performed to evaluate the prediction accuracy of these models by calculating the absolute deviation between the predicted and the true phantom movement as follows:

$$D(t) = L_2(\overrightarrow{v_p}(t) - \overrightarrow{v_r}(t)) \tag{13}$$

where $D(t)$ was the absolute deviation between $\overrightarrow{v_p}(t)$ and $\overrightarrow{v_r}(t)$, which were the predicted and true phantom movement at time t, respectively. $\overrightarrow{v_p}(t)$ can be obtained using Eq. 9, and $\overrightarrow{v_r}(t)$ can be measured directly using the EM position sensor attached to the phantom. L_2 is the Euclidean distance.

Clinical study

Clinical study was carried out on eight volunteers (Table 1, where BMI stand for Body Mass Index). Data from subject 7 were discarded because his liver was much higher than others in abdominal cavity, which made it impossible to capture UITS-RMS set for training the liver motion model.

Considering that a large portion of the liver is located in the right hypochondriac region, we placed the EM position sensor within the area enclosed by umbilicus, xiphoid, left arcus costalis and the umbilicus horizontal line (Fig. 6). So the skin movement could be detected, whereas the probe pressure effect was minimized as far as possible. 'UITS-RMS set' was captured from sagittal plane of the left liver to train the subject-specific liver motion model when the experienced clinician held the probe steady and perpendicular to the ground. In general, ultrasound image frames of liver with features such as vessels were acquired over 3–5 breathing cycles.

Table 1 Profile of 8 subjects

Subject	Gender	Age	Weight/kg	Height/cm	BMI
1	M	25	54	160	21.09
2	M	23	65	175	21.22
3	M	30	65	170	22.49
4	M	27	62	174	20.48
5	M	25	70	185	20.45
6	M	24	75	183	22.40
7	M	30	79	182	23.85
8	M	25	55	170	19.03

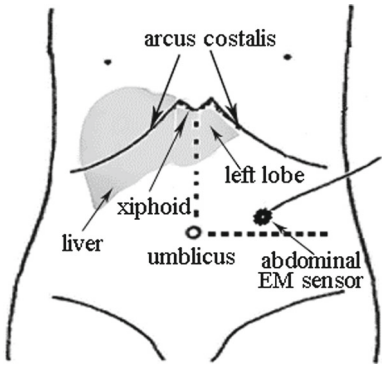

Fig. 6 The abdominal EM position sensor used to track respiratory motion signal was placed within the area enclosed by umbilicus, xiphoid, left arcus costalis and the umbilicus horizontal line. The ultrasound image frames used to track liver motion were captured from sagittal section of left liver

At the stage of modeling, HHS UITS-RMS set was used to build liver motion model. For each subject, at least two HHS UITS-RMS datasets were captured to build motion models. These models were then compared from the view of the slope along SI, AP (Anterior–Posterior) and LR (Left–Right) axes to evaluate the operator dependency of the modeling process.

In clinical study, abdominal skin of the subject mainly moved along a single axis (AP axis). The translation component of abdominal EM sensor's position with the maximal amplitude over time of $\vec{P}_t$ was obtained straightforwardly, by comparing the amplitudes of the 3 translation components. Compared to PCA-based approach, the maximal component-based approach was easy to implement. Robustness of these two approaches was analyzed to choose a more reliable measurement of respiratory depth.

To eliminate the influence of probe translation and rotation, ultrasound image frames of 3–5 breathing cycles with the translation amplitude of at most 2 mm and the rotation amplitude of at most 2 degree were selected from the UITS-RMS set to track internal liver motion.

Visual inspections were performed by clinician to evaluate the effectiveness qualitatively. The consistency of identical structures, such as liver capsule and vessels, in the fused

images with/without motion compensation was used to evaluate the model performance in real-time fusion imaging, as well as offline assessment (Fig. 11). Quantitative analysis of fusion error reduction included manually measuring misalignment of identical features such as vessel cross section and vessels bifurcation in fusion images (with/without liver motion compensation) by:

$$\varepsilon = L_2(\overrightarrow{P_{\text{us}}} - \overrightarrow{P_{\text{MRI}}}) \tag{14}$$

where ε was misalignment (fusion error) of identical feature in ultrasound image ($\overrightarrow{P_{\text{us}}}$) and corresponding MRI slice ($\overrightarrow{P_{\text{MRI}}}$).

Out of all image frames, max respiratory motion-induced fusion error was determined by the respiratory depth which was the most distant from the registration.

Results

Phantom study

Figure 7 illustrates the phantom motion model of simulated motion along the SI, AP and LR axes using HHS UITS-RMS set. It can be seen that the motion model was mainly along SI axis. This was consistent with the fact that the phantom was driven to move along the SI axis.

Visual inspections show that the consistency of identical structures, such as liver capsule and vessel, was significantly improved when liver motion was corrected using the online model.

Table 2 shows prediction errors in phantom study. It can be seen that there was only a marginal difference in prediction error between the models built on FEF and HHS UITS-RMS sets. For FEF and HHS groups, the probe still moved and rotated a little, because of the phantom's movement. The prediction error for the HHR-AP group was the minimal. This might be explained by the fact that when the probe rotated around AP axis, more liver motion could be captured compared to other groups. HHTRR group had the maximal prediction error. This was due to the fact that the probe was too far away from the sagittal slice and there was too much movement when probe translation and rotation were both introduced. These factors made HHTRR group prone to error when tracking liver motion.

To summarize, the proposed method could effectively compensate for the respiratory live motion using the subject-specific model in phantom study. Since it is hard for the clinician to keep hand steady, HHS is advised to capture the UITS-RMS set in clinical study and clinically.

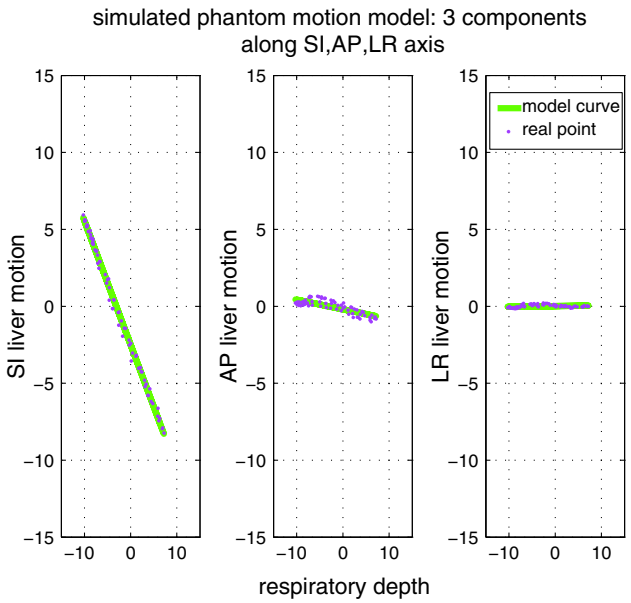

Fig. 7 The phantom motion model of simulated movement along its SI, AP and LR axes using HHS UITS-RMS set. *Purple dots* indicate the position of liver phantom computed using ultrasound image frames, *green lines* indicate the SI, AP and LR components of the motion model

Clinical study

Modeling

Respiratory mapping Typical respiratory motion senor's positions are displayed in Fig. 8a. The component with the maximum amplitude (x axis) was determined visually. Respiratory depth obtained using these two approaches were compared in Fig. 8b.

There was very little difference between the two formulae when the EM field generator was placed to make the xy plane of EM field parallel to body sagittal plane. However, the component scale of the respiratory sensor's motion heavily depended on the pose of the EM field generator. Thus, the PCA-based approach was much more robust. Therefore, the projection on the first primary component of PCA was used as the respiratory depth.

Model building The subject-specific liver motion model is shown in Fig. 9. The difference between the models of 7 subjects is compared in Fig. 10.

In Fig. 9, it can be seen that a strong linear relationship existed between respiratory depth and liver motion. Liver displacement along SI axis was about 12 mm. Therefore, fusion error could be as large as 12 mm for this subject if no motion compensation was performed.

Figure 10 compares the SI components of the subject-specific liver models for 7 subjects, which were built using each subject's UITS-RMS set. Among different subjects, the

Table 2 Prediction accuracy of phantom study

	Probe translation (mm)			Probe rotation (degree)			Respiratory motion model			Prediction Error mean ± SD (mm)
	SI	AP	LR	SI	AP	LR	SI	AP	LR	
FEF	2	2	2	0.6	0.6	0.6	0.86	−0.05	−0.04	1.0 ± 0.7
HHS	4	3	6	2	2	2	0.85	0.00	0.03	1.2 ± 0.6
HHR-SI	3	4	9	5	1.5	1	0.90	−0.02	−0.01	0.7 ± 0.5
HHR-AP	21	6	7	2	9	3	1.05	−0.33	0.01	0.3 ± 0.2
HHTRR	25	18	12	8	14	18	0.46	−0.06	1.26	4.2 ± 1.4

Probe translation and rotation represent the probe's motion range for the ultrasound image sequence. The respiratory liver motion model consists of 3 components along SI, AP and LR axes. The model's prediction error is showed in the last column

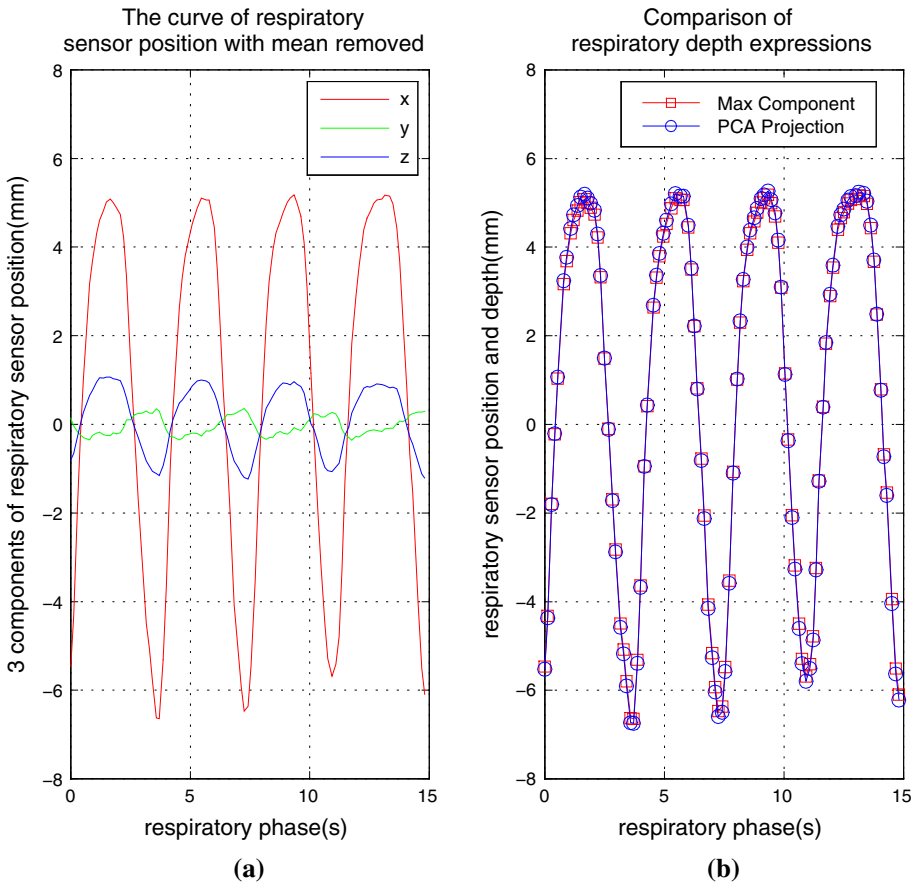

Fig. 8 Comparison of respiratory depths represented by maximal and PCA component. **a** The 3 components of the abdominal respiratory sensor position. **b** The overlay of these two representations of respiratory depth

liver motion along SI axis ranged from 6.0 to 14.4 mm, and the respiratory depth ranged from 5.8 to 13.6 mm. Therefore, a subject-specific liver motion model is needed for each individual.

Table 3 shows the deviation of motion models based on at least two groups of HHS UITS-RMS set for each subject. Maximum slope difference was along SI axis. SI component difference of compensation vectors, which were obtained using different motion models of one subject, was 0.95 ± 0.65 mm when the respiratory depth was 10 mm. It indicated that the operator dependency was not too high.

Real-time motion compensation

Figure 11 demonstrates the qualitative fusion errors correction in four liver sections. Key anatomical features, labeled by 'A–H,' were evaluated. Table 4 shows the misalignment of these features for 7 subjects, as well as the residual error rate after compensation.

In Fig. 11, the top row is the ultrasound images captured from different liver sections in this study. The second row is the MRI images at the same location from the uncompensated 3D MRI dataset. The corresponding fusion images in

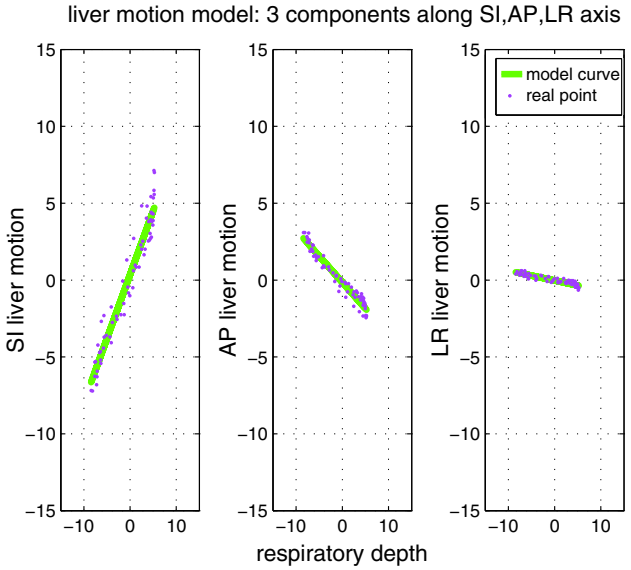

Fig. 9 A typical motion model in clinical study along the volunteer's SI, AP and LR axes, using the same definition as Fig. 7

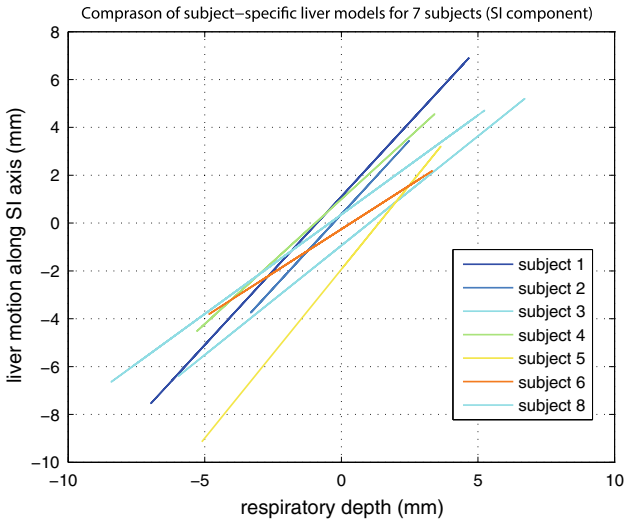

Fig. 10 Comparison of the SI components of the subject-specific liver models for 7 subjects. Respiratory depth, liver motion along SI axis and the SI slope of model varied among subjects

the third row demonstrate the obvious misalignment of identical vessel structures and liver capsule in ultrasound and uncompensated MRI images. And some vessel is missing in the uncompensated MRI slice, compared to the ultrasound image (Fig. 11 (3-a)-(3-c), F). The fourth row is the MRI slice extracted from the compensated 3D MRI images using proposed model. The fusion images using the compensated MRI image at the bottom row show that the proposed model effectively corrected the fusion errors by reducing the distances of identical vessel structures and liver capsule between ultrasound frame and compensated MRI slice, and improving the consistency of liver structures in both modalities to a great extent. Table 4 summarizes the quantitative evaluation of fusion error from all subjects. The ratio of motion-compensated fusion error to the original error varied from 10 (0.96/9.40 mm) to 28 % (2.90/10.22 mm).

Table 3 The deviation of motion models of each subject based on HHS UITS-RMS sets captured at different time in one experiment

Subject	SI	AP	LR
1	0.155	0.172	0.004
2	0.017	0.039	0.019
3	0.130	0.018	0.037
4	0.176	0.040	0.021
5	0.115	0.046	0.003
6	0.057	0.039	0.070
8	0.017	0.028	0.085
Mean ± SD	0.095 ± 0.065	0.055 ± 0.053	0.034 ± 0.032

They were compared from the view of the slope difference along SI, AP and LR axes to evaluate the operator dependency of modeling process

Discussion

This paper developed an online subject-specific liver motion model using an EM position sensor and 2D ultrasound image frames. Phantom study and clinical study showed that the proposed model could correct the fusion errors induced by respiratory movement effectively. In phantom study, the consistency of identical structures such as liver capsule and vessels was improved significantly when simulated liver motion was corrected using the online model, and the prediction error of HHS group was 1.2 ± 0.6 mm. Clinical study demonstrated that fusion error was significantly reduced. The ratio of motion-compensated fusion error to the original non-motion-compensated error varied from 10 (0.96/9.40 mm) to 28 % (2.90/10.22 mm).

Currently adopted respiratory gating-like method in ultrasound-MRI/CT fusion imaging highly relies on subject cooperativeness. It prolongs the surgery time and decreases the effectiveness and reliability of operation. In comparison to the 4D model [23–26], our method did not require 4D dataset. Online model construction was easy, fast, with less cost. Compared with the indirect respiratory heart motion correction approach [27], we predicted liver motion based on liver ultrasound images. Instead of using the average motion compensation of selected 2D ultrasound frames as proposed by other researchers [6], our method corrected the liver motion based on the exact current ultrasound image. In this paper, speckle tracking technique was employed to get more precise liver motions quickly, and linear fitting was used to suppress the outliers and to improve the model precision. Our 2D liver sagittal plane translation model was able

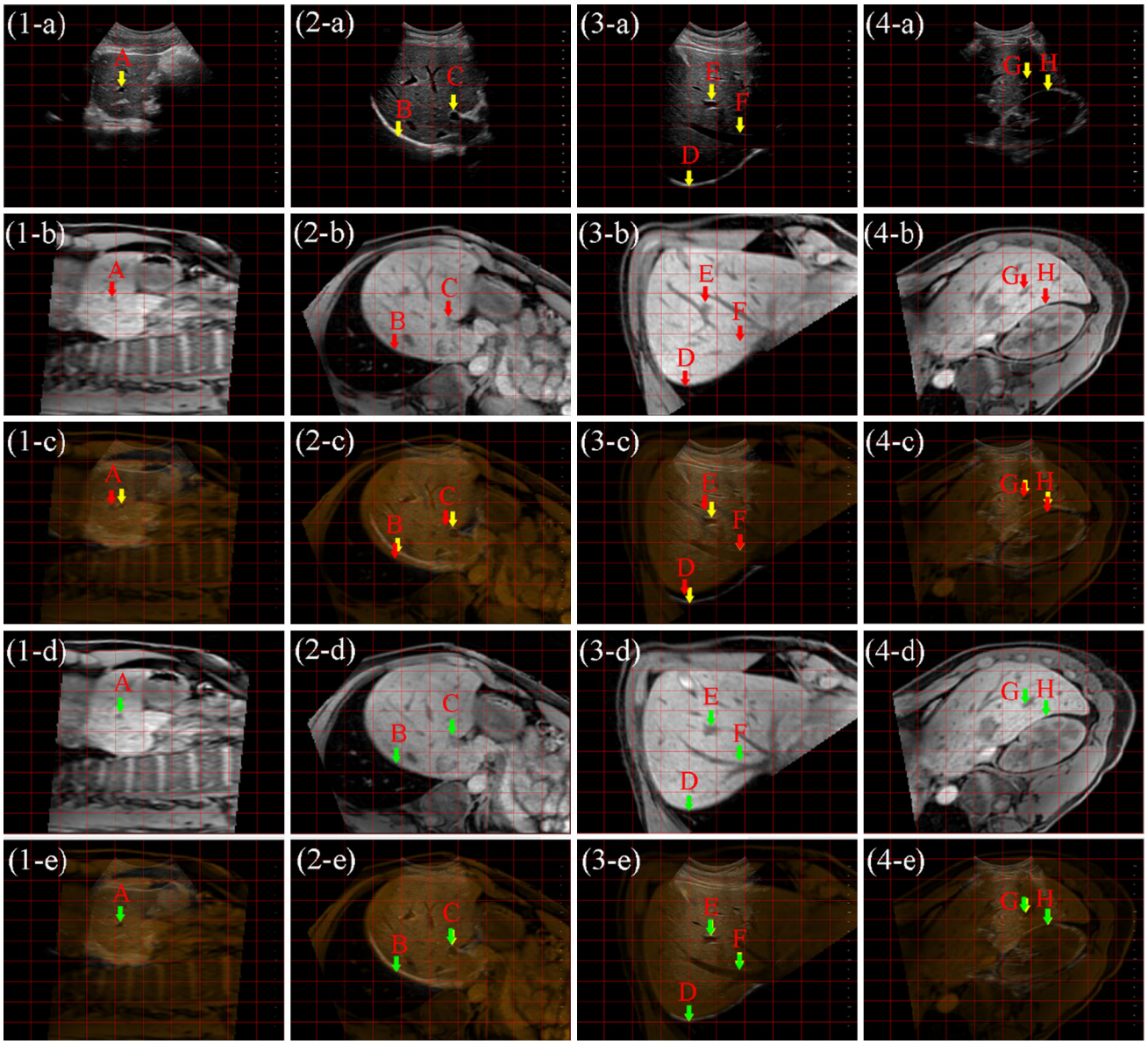

Fig. 11 Compensation performance of the proposed liver motion prediction model. *Top row* is ultrasound slice, *second* and *third rows* are corresponding uncompensated MRI slice and its fusion display with ultrasound slice. The *fourth* and *fifth rows* are corresponding compensated MRI slice, and its fusion display. *Each column* is slices extracted from the sagittal slice of left liver (*1*), parallel intercostal (*2*), hepatic portal vein (*3*) and vertical intercostal (*4*). The *yellow arrows* indicate the inner structures or the liver capsule (A–H) in the ultrasound image, the *red arrows* indicate the corresponding features in uncompensated MRI slice, and the *green arrows* indicate the corresponding features in compensated MRI slice

to compensate liver motion by at least 72 % (1–28 %), which is similar to Wein's finding [29].

However, our study has limitations. The proposed method compensated for current respiratory liver motion with respect to the registered respiratory phase. The compensation effect was dependent on the accuracy of the registration to a large scale. If the registration error was unacceptable, the fusion errors could not be reduced effectively. Currently, the 2D–3D registration of 2D ultrasound and 3D MRI/CT was performed manually, which was slow and operator-dependent. Moreover, this method was not suitable for the person whose liver located too high in abdominal cavity, because UITS-RMS set would be hard to obtain. All subjects in this paper were healthy with normal BMI. No patient was included.

Consequently, UITS-RMS sets of liver in parallel and vertical intercostal plane are needed in addition to that of liver sagittal plane to reconstruct more accurate liver motion. The semi-automatic registration of 2.5D ultrasound-3D MRI/CT

Table 4 Fusion errors with/without liver motion compensation using the proposed model (subject 7 is discarded)

	Subject 1	Subject 2	Subject 3	Subject 4	Subject 5	Subject 6	Subject 8
Left lobe							
Before	9.40 (1.09)	10.24 (4.77)	5.41 (0.78)	8.15 (0.20)	7.11 (0.32)	9.44 (0.19)	12.43 (2.08)
After	0.96 (0.01)	1.52 (0.02)	0.77 (0.81)	1.01 (0.48)	1.71 (1.22)	1.98 (1.46)	1.88 (0.36)
Residual	10 %	15 %	14 %	12 %	24 %	21 %	15 %
Hepatic portal vein							
Before	8.42 (1.37)	8.25 (1.93)	14.42 (3.15)	8.15 (0.18)	7.72 (0.46)	9.29 (3.20)	16.07 (2.11)
After	0.92 (0.45)	1.09 (0.59)	2.46 (0.78)	1.42 (0.73)	1.39 (0.21)	2.05 (0.34)	3.18 (1.06)
Residual	11 %	13 %	17 %	17 %	18 %	22 %	20 %
Parallel intercostal							
Before	5.89 (0.64)	7.39 (0.21)	4.63 (1.56)	11.97 (0.12)	7.16 (1.06)	12.05 (0.91)	9.53 (3.53)
After	1.07 (0.90)	1.36 (0.21)	0.64 (0.05)	2.28 (0.63)	1.24 (0.80)	1.72 (0.26)	1.28 (0.10)
Residual	18 %	18 %	13 %	19 %	17 %	14 %	13 %
Vertical intercostal							
Before	13.93 (1.08)	8.33 (2.39)	10.22 (1.07)	8.51 (0.09)	12.92 (0.33)	7.21 (1.45)	11.23 (1.00)
After	1.63 (0.18)	1.69 (0.21)	2.90 (2.35)	1.51 (1.53)	2.30 (2.30)	1.51 (0.60)	2.28 (0.21)
Residual	12 %	20 %	28 %	17 %	18 %	21 %	20 %
Liver–kidney interface							
Before	8.50 (1.72)	6.46 (0.51)	–	–	–	–	–
After	1.76 (0.20)	0.81 (0.20)	–	–	–	–	–
Residual	21 %	13 %	–	–	–	–	–

The fusion error, mean (standard deviation), was the manually measured distance (in mm) between the identical liver structures in ultrasound and MRI images before and after motion compensation. The residual was defined as the ratio of motion-compensated fusion error to the original error. Measurement of liver–kidney interface was only obtained from subject 1 & 2

will be developed to improve the registration accuracy. Furthermore, direct tracking of abdominal skin, instead of indirect measurement using additional position sensor will be investigated in the future. More subjects with wider range of BMI will be included to validate the feasibility of this method. The performance of this method in fusion errors reduction for kidney motion compensation will be tested as well.

Conclusion

This paper has proposed an online subject-specific modeling and real-time compensation method to compensate for the respiratory liver motion, thereby reducing the relevant fusion errors in liver ultrasound-MRI/CT fusion imaging using a skin position sensor and 2D ultrasound image frames. Clinical study demonstrates that this model could compensate for respiratory liver motion effectively. The proposed method is feasible to realize real-time fusion imaging during smooth respiration. It may provide surgeons with stable multimodality fusion images with acceptable accuracy in real time. This method could potentially correct fusion error caused by respiratory movement in kidney fusion imaging.

Acknowledgments This work was supported in part by grants from National Basic Research Program of China (2011CB707701), and National Natural Science Foundation of China (61361160417, 81271735, 81127003).

Conflict of interest None.

References

1. Trobaugh JW, Kessman P, Dietz D, Bucholz R (1997) Ultrasound in image fusion: a framework and applications. Ultrasonics Symposium, 1997 Proceedings, 1997 IEEE 2:1393–1396. doi:10.1109/ULTSYM.1997.661837
2. Nakai M, Sato M, Sahara S, Takasaka I, Kawai N, Minamiguchi H, Tanihata H, Kimura M, Takeuchi N (2009) Radiofrequency ablation assisted by real-time virtual sonography and CT for hepatocellular carcinoma undetectable by conventional sonography. Cardiovasc Interv Radiol 32(1):62–69
3. Marks L, Young S, Natarajan S (2013) MRI-ultrasound fusion for guidance of targeted prostate biopsy. Curr Opin Urol 23(1):43–50. doi:10.1097/MOU.0b013e32835ad3ee
4. Stang A, Keles H, Hentschke S, Seydewitz C, Keuchel M, Pohland C, Dahlke J, Weilert H, Wessling J, Malzfeldt E (2010) Real-time ultrasonography-computed tomography fusion imaging for staging of hepatic metastatic involvement in patients with colorectal cancer: initial results from comparison to US seeing separate CT images and to multidetector-row CT alone. Investig Radiol 45(8):491–501
5. Beller S, Hunerbein M, Eulenstein S, Lange T, Schlag PM (2007) Feasibility of navigated resection of liver tumors using multiplanar

visualization of intraoperative 3-dimensional ultrasound data. Ann Surg 246(2):288–294. doi:10.1097/01.sla.0000264233.48306.99
6. Xu S, Kruecker J, Turkbey B, Glossop N, Singh AK, Choyke P, Pinto P, Wood BJ (2008) Real-time MRI-TRUS fusion for guidance of targeted prostate biopsies. Comput Aided Surg 13(5):255–264
7. Clevert D, Paprottka P, Helck A, Reiser M, Trumm C (2012) Image fusion in the management of thermal tumor ablation of the liver. Clin Hemorheol Microcirc 52(2):205–216
8. Helck A, D'Anastasi M, Notohamiprodjo M, Thieme S, Sommer W, Reiser M, Clevert DA (2012) Multimodality imaging using ultrasound image fusion in renal lesions. Clin Hemorheol Microcirc 50(1–2):79–89. doi:10.3233/CH-2011-1445
9. Ewertsen C, Hansen KL, Henriksen BM, Nielsen MB (2012) Improving accuracy for image fusion in abdominal ultrasonography. Diagnostics 2(4):34–41. doi:10.3390/diagnostics2030034
10. Nicolau S, Pennec X, Soler L, Ayache N (2007) Clinical evaluation of a respiratory gated guidance system for liver punctures. In: Medical image computing and computer-assisted intervention-MICCAI 2007. Springer, Berlin, pp 77–85
11. Wunderink W, Mendez Romero A (2008) Reduction of respiratory liver tumor motion by abdominal compression in stereotactic body frame, analyzed by tracking fiducial markers implanted in liver. Int J Radiat Oncol Biol Phys 71(3):907–915. doi:10.1016/j.ijrobp.2008.03.010
12. Remouchamps VM, Letts N, Vicini FA, Sharpe MB, Kestin LL, Chen PY, Martinez AA, Wong JW (2003) Initial clinical experience with moderate deep-inspiration breath hold using an active breathing control device in the treatment of patients with left-sided breast cancer using external beam radiation therapy. Int J Radiat Oncol Biol Phys 56(3):704–715
13. Biro P, Spahn D, Pfammatter T (2009) High-frequency jet ventilation for minimizing breathing-related liver motion during percutaneous radiofrequency ablation of multiple hepatic tumours. Br J Anaesth 102(5):650–653
14. Kothary N, Heit JJ, Louie JD, Kuo WT, Loo BW Jr, Koong A, Chang DT, Hovsepian D, Sze DY, Hofmann LV (2009) Safety and efficacy of percutaneous fiducial marker implantation for image-guided radiation therapy. J Vasc Interv Radiol 20(2):235–239
15. Schweikard A, Shiomi H, Adler J (2005) Respiration tracking in radiosurgery without fiducials. Int J Med Robot Comput Assist Surg 1(2):19–27
16. Hakime A, Barah A, Deschamps F, Farouil G, Joskin J, Tselikas L, Auperin A, de Baere T (2013) Prospective comparison of freehand and electromagnetic needle tracking for US-guided percutaneous liver biopsy. J Vasc Interv Radiol 24(11):1682–1689
17. Volumetric Measurement and Image Fusion. Ascension Technology Corporation. http://www.ascension-tech.com/medical/volumetric.php. Accessed 29 Jan 2012
18. iU22 xMATRIX Ultrasound System with PercuNav. Philips. http://www.healthcare.philips.com/main/products/ultrasound/systems/percunav/percunav_iu22.wpd. Accessed 2 Sept 2013
19. SMART FUSION. http://www.myaplio.com/smartfusion/. Accessed 26 Nov 2013
20. GE Healthcare Introduces Ultrasound Fusion; New LOGIQ E9 Merges Real-time Ultrasound with CT, MR AND PET. (2008) GE Healthcare.http://www.newswire.ca/fr/story/344723/ge-healthcare-introduces-ultrasound-fusion-new-logiq-e9-merges-real-time-ultrasound-with-ct-mr-and-pet. Accessed 7 Dec 2013
21. Fusion of Images: CT and Ultrasound Combined. (2012) SIEMENS. http://www.siemens.com/innovation/en/news/2012/e_inno_1201_2.htm. Accessed 26 Nov 2013
22. Zhu L, Ding H, Zhu L, Wang G (2011) A robust registration method for real-time ultrasound image fusion with pre-acquired 3D dataset. In: Conference proceedings: annual international conference of the IEEE engineering in medicine and biology society IEEE engineering in medicine and biology society conference 2011, pp 2638–2641. doi:10.1109/IEMBS.2011.6090727
23. Khamene A, Warzelhan JK, Vogt S, Elgort D, Chefd'Hotel C, Duerk JL, Lewin J, Wacker FK, Sauer F (2004) Characterization of internal organ motion using skin marker positions. In: Medical image computing and computer-assisted intervention-MICCAI 2004. Springer, New York, pp 526–533
24. Blackall JM, Penney GP, King AP, Hawkes DJ (2005) Alignment of sparse freehand 3-D ultrasound with preoperative images of the liver using models of respiratory motion and deformation. IEEE Trans Med Imaging 24(11):1405–1416
25. He T, Xue Z, Xie W, Wong ST (2010) Online 4-D CT estimation for patient-specific respiratory motion based on real-time breathing signals. In: Medical image computing and computer-assisted intervention-MICCAI 2010. Springer, New York, pp 392–399
26. Tanner C, Boye D, Samei G, Szekely G (2012) Review on 4D models for organ motion compensation. Crit Rev^{TM} Biomed Eng 40(2)
27. Atkinson D, Burcher M, Declerck J, Noble JA (2001) Respiratory motion compensation for 3-D freehand echocardiography. Ultrasound Med Biol 27(12):1615–1620
28. De Silva T, Fenster A, Bax J, Gardi L, Romagnoli C, Samarabandu J, Ward AD (2012) 2D–3D rigid registration to compensate for prostate motion during 3D TRUS-guided biopsy. SPIE Medical Imaging:83160O–83160O-83166
29. Wein W, Cheng J-Z, Khamene A (2008) Ultrasound based respiratory motion compensation in the abdomen. MICCAI 2008 Worshop on Image Guidance and Computer Assistance for Softissue Intervetions 32(6):294
30. Blackall J, Ahmad S, Miquel M, McClelland J, Landau D, Hawkes D (2006) MRI-based measurements of respiratory motion variability and assessment of imaging strategies for radiotherapy planning. Phys Med Biol 51(17):4147
31. Rohlfing T, Maurer CR Jr, O'Dell WG, Zhong J (2004) Modeling liver motion and deformation during the respiratory cycle using intensity-based nonrigid registration of gated MR images. Med Phys 31:427
32. Brandner ED, Wu A, Chen H, Heron D, Kalnicki S, Komanduri K, Gerszten K, Burton S, Ahmed I, Shou Z (2006) Abdominal organ motion measured using 4D CT. Int J Radiat Oncol Biol Phys 65(2):554–560
33. Yang M, Ding H, Wang X, Wang G (2014) An analysis of respiration induced liver motion mode. J Zhejiang Univ (Engineering Science) 48(9) (in press)
34. Gierga DP, Brewer J, Sharp GC, Betke M, Willett CG, Chen GT (2005) The correlation between internal and external markers for abdominal tumors: implications for respiratory gating. Int J Radiat Oncol Biol Phys 61(5):1551–1558
35. Ernst F, Bruder R, Schlaefer A, Schweikard A (2012) Correlation between external and internal respiratory motion: a validation study. Int J Comput Assist Radiol Surg 7(3):483–492. doi:10.1007/s11548-011-0653-6
36. De Groote A, Wantier M, Chéron G, Estenne M, Paiva M (1997) Chest wall motion during tidal breathing. J Appl Physiol 83(5):1531–1537
37. Li PC, Lee WN (2002) An efficient speckle tracking algorithm for ultrasonic imaging. Ultrason Imaging 24(4):215–228
38. Shlens J (2005) A tutorial on principal component analysis. Systems Neurobiology Laboratory, University of California at San Diego 82
39. Yeung F, Levinson SF, Parker KJ (1998) Multilevel and motion model-based ultrasonic speckle tracking algorithms. Ultrasound Med Biol 24(3):427–441